A MESHLESS SINGULAR HYBRID BOUNDARY NODE METHOD FOR 2-D ELASTOSTATICS

Hong-Tao Wang, Zhen-Han Yao*, and Song Cen

ABSTRACT

As a boundary-type meshless method, the HBNM presented by authors' group is based on a modified variational principle and MLS approximation, so it possesses the advantages of both BEM and meshless methods. This method does not require any mesh for variable interpolations or for boundary integration. In order to avoid the singular integrals which exist in HBNM, the RHBNM was proposed, in which the source points of the fundamental solutions are moved outside the domain. However, such treatment is not convenient for problems with irregular geometries and may lead to insufficient numerical stability. In this paper, the singular integral and the "boundary layer effect" in HBNM are properly treated. Thus, the dependence of the numerical results on scale factor in RHBNM can be successfully avoided. Numerical examples show high accuracy and high convergence rates for the presented scheme.

Key Words: meshless method, singular approach, hybrid boundary node method.

I. INTRODUCTION

The two most important and effective numerical methods in engineering analysis are the Finite Element Method and the Boundary Element Method. However, the reliance on meshes in these two mesh-based methods leads to some unavoidable drawbacks. On one hand, mesh generation is an arduous, burdensome and time-consuming task in 3-D problems with complicated irregular shapes. On the other hand, much difficulty emerges, while solving problems associated with extremely large deformations or problems involving frequent re-meshing, such as crack propagation. In recent years, several meshless methods have been proposed to avoid the pitfalls mentioned above. These novel methods include Smooth Particle Hydrodynamics (Lucy, 1977), Diffuse Element method (Nayroles *et al*., 1992), Element Free Galerkin (EFG) method (Belytschko *et al*., 1994; 1996), Reproducing Kernel Particle Method (Liu *et al*., 1995), Meshless Local Petrov-Galerkin (MLPG) method (Atluri and Zhu, 1998; 2000; Atluri *et al*., 1999), Local Boundary Integral Equation (LBIE) method (Zhu *et al*., 1998; Atluri *et al*., 2000), Boundary Node Method (BNM) (Mukherjee and Mukherjee, 1997; Kothnur *et al*., 1999) and so on. In authors' group, a meshless method, called Hybrid Boundary Node Method (HBNM) has been presented (Zhang *et al*., 2002).

EFG is based on a global symmetric weak form like conventional FEM, and using the Moving Least Squares (MLS) approximation to construct the shape functions. Though the use of MLS leads to the fact that no mesh is required in this method for the interpolation of the variables, the background cells are still inevitable for the weak form integration.

The concept of local symmetric and unsymmetric weak forms over a local sub-domain was proposed in LBIE and MLPG. Since sub-domains are used for the integration of the local weak forms, no mesh or cell is needed anymore. In further studies, Atluri and his co-workers explored several kinds of trial and test functions in the MLPG method and six types of MLPG method were obtained (Atluri and Shen, 2002).

In BNM, the MLS approximation is introduced into Boundary Integral Equations (BIE). Though only a nodal data structure on the bounding surface of a

*Corresponding author. (Tel: +8610-62772913; Fax: +8610-62781824; Email: demyzh@tsinghua.edu.cn)

H. T. Wang, Z. H. Yao, and S. Cen are with the Department of Engineering Mechanics, Tsinghua University, Beijing, 100084 P.R. China.

body is needed in this method, an underlying cell structure on the boundary is still inevitable for numerical integration.

The HBNM is a boundary-type meshless method presented by coupling a modified variational principle and the MLS approximation. This method possesses the attractive meshless character of MLS as well as the dimension-reduction advantage of BEM, i.e., only some scattered nodes distributed on the boundary of the solution domain are needed for the discretization of the whole structure. Similar to the MLPG and LBIE, this method does not require any mesh or cell for variable interpolations or for numerical integration.

In order to avoid the singular integrals in HBNM, a Regular Hybrid Boundary Node Method (RHBNM) is proposed (Zhang and Yao, 2001a; 2001b), in which the source points of the fundamental solutions are moved outside the domain. This method has been successfully used in solving 2-D and 3-D potential problems, 2-D and 3-D linear elasticity (Zhang *et al*., 2003; Zhang and Yao, 2004), including 2-D thin structures (Zhang and Yao, 2002). However, such regularization treatment may lead to some problems: the results are dependent on the choice of the scale factor or the assignment of the source points; it is not convenient to solve the problems with a concave boundary or a crack; the numerical stability is insufficient sometimes.

To avoid these problems, a new singular scheme for the HBNM is proposed in this paper, where the singular integrals are appropriately approached by using an approach similar to that of BEM. Numerical examples show that the new SHBNM is more robust than the RHBNM.

The BIE in SHBNM is derived from the modified variational functional in Section II. The variable interpolation using MLS approximation and fundamental solutions are described in Sections III and IV, respectively. A system of algebraic equations is given in Section V. The approach to singular integrals is discussed in Section VI. Finally, several numerical examples are presented in Section VII.

II. BOUNDARY INTEGRAL EQUATION

The governing equation and the corresponding boundary conditions of the two-dimensional linear elasticity problem without body forces can be written as follows:

$$\begin{aligned} &\sigma_{ij}(\boldsymbol{u}),_j=0 && \text{in } \Omega \\ &u_i=\overline{u}_i && \text{on } \Gamma_u \\ &t_i\equiv\sigma_{ij}(\boldsymbol{u})n_j=\overline{t}_i && \text{on } \Gamma_t \end{aligned} \tag{1}$$

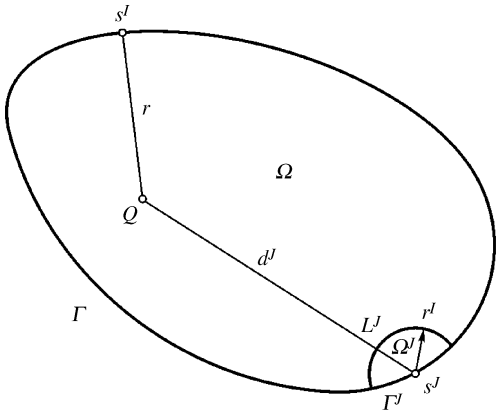

Fig. 1 The local sub-domain centered at a field point s^J and the source point s^I

where Ω is the global domain enclosed by the boundary $\Gamma=\Gamma_u+\Gamma_t$, $\sigma_{ij}(\boldsymbol{u})$ denote the stresses corresponding to the displacement field $\boldsymbol{u}$ with components u_i, $\overline{u}_i$, the prescribed displacements on the displacement boundary Γ_u, $\overline{t}_i$, the prescribed tractions on the traction boundary Γ_t, and n_i, the unit outward normal vector to the boundary Γ.

The corresponding weak form of integral equations governing in a sub-domain can be written as (Zhang *et al.*, 2003):

$$\int_{\Gamma^J+L^J}(t_i-\tilde{t}_i)v^J d\Gamma-\int_{\Omega^J}\sigma_{ij}(\boldsymbol{u}),_j v^J d\Omega=0 \tag{2}$$

$$\int_{\Gamma^J+L^J}(u_i-\tilde{u}_i)v^J d\Gamma=0 \tag{3}$$

where Ω^J is a sub-domain, which is deliberately chosen as the intersection of the global domain Ω and a circle centered at a node s^J on the boundary Γ (Fig. 1), Γ^J and L^J are its boundaries; v^J is the test function, u_i, the displacement field inside the domain, $\tilde{u}_i$, the boundary displacements, $\tilde{t}_i$, boundary tractions. u_i, $\tilde{u}_i$ and $\tilde{t}_i$ are taken as three independent variables. And $\tilde{u}_i$ satisfies the displacement boundary conditions, i.e., $\tilde{u}_i=\overline{u}_i$ on Γ_u.

In order to get rid of the boundary integrals over L^J, the test function v^J is chosen appropriately, such as the Gaussian weight function or 4th-order spline weight function in the MLS approximation, or the compactly supported positive definite radial basis functions (Atluri and Shen, 2002; Wu, 1995).

Thus, Eqs. (2) and (3) can be rewritten as:

$$\int_{\Gamma^J}(t_i-\tilde{t}_i)v^J d\Gamma-\int_{\Omega^J}\sigma_{ij}(\boldsymbol{u}),_j v^J d\Omega=0 \tag{4}$$

$$\int_{\Gamma^J}(u_i-\tilde{u}_i)v^J d\Gamma=0 \tag{5}$$

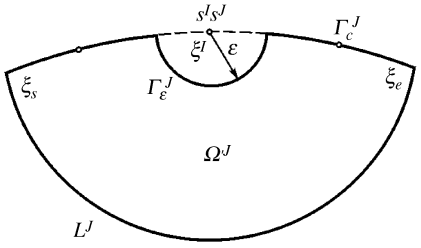

Fig. 2 Modified sub-domain centered at the field point s^J and source point s^I (s^J and s^I are coincident)

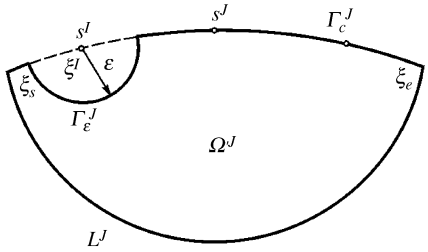

Fig. 3 Modified sub-domain centered at the field point s^J and source point s^I (s^J and s^I are not coincident)

III. MLS APPROXIMATION

The MLS approximation in HBNM is independently constructed on the piecewise smooth segments Γ^k, k=1, 2, ⋯, M, using curvilinear coordinates. This approximation scheme for the boundary displacement $\tilde{u}_i$ and boundary traction $\tilde{t}_i$ are independently defined as

$$\tilde{u}_i(s) = \sum_{I=1}^{N} \Phi^I(s)\hat{u}_i^I \tag{6}$$

$$\tilde{t}_i(s) = \sum_{I=1}^{N} \Phi^I(s)\hat{t}_i^I \tag{7}$$

where

$$\Phi^I(s) = \sum_{j=1}^{m} p^j(s)[\boldsymbol{A}^{-1}(s)\boldsymbol{B}(s)]^{jI} \tag{8}$$

$$\boldsymbol{A}(s) = \sum_{I=1}^{N} w^I(s)\boldsymbol{p}(s^I)\boldsymbol{p}^T(s^I) \tag{9}$$

$$\boldsymbol{B}(s)=[w^1(s)\boldsymbol{p}(s^1),\ w^2(s)\boldsymbol{p}(s^2),\ \ldots,\ w^N(s)\boldsymbol{p}(s^N)] \tag{10}$$

In the above equations, $\boldsymbol{p}$ is a complete monomial basis vector, and the weight function $w^I(s)$ is chosen as the Gaussian weight function:

$$w^I(s)=\begin{cases} \dfrac{\exp[-(d^I/c^I)^2]-\exp[-(\hat{d}^I/c^I)^2]}{1-\exp[-(\hat{d}^I/c^I)^2]} & 0 \le d^I \le \hat{d}^I \\ 0 & d^I \ge \hat{d}^I \end{cases} \tag{11}$$

where $d^I=|s-s^I|$, the distance from a point s to the boundary node s^I, measured along Γ^k; $\hat{d}^I$ is the support size of the weight function; c^I is a parameter controlling the shape of the weight function.

Since the MLS approximation does not possess the Kronecker Delta property, $\hat{u}_i^I$ and $\hat{t}_i^I$ should be obtained first, while the boundary conditions are imposed. For a well-posed problem, the value of either u_i or t_i is known on the boundary. Thus, $\hat{u}_i^I$ on Γ_u and $\hat{t}_i^I$ on Γ_t can be obtained as

$$\hat{u}_i^I = \sum_{J=1}^{N} R^{IJ}\overline{u}_i^J \tag{12}$$

$$\hat{t}_i^I = \sum_{J=1}^{N} R^{IJ}\overline{t}_i^J \tag{13}$$

where N is the number of boundary nodes on an edge; $R^{IJ}=[\Phi^J(s^I)]^{-1}$. More detail can be seen in (Zhang *et al.*, 2003).

IV. FIELD VARIABLES INTERPOLATION

Like the hybrid BEM model in (DeFigueredo and Brebbia, 1989), the displacement field u_i inside the global domain and on the boundary Γ can be defined as

$$u_i = \sum_{I=1}^{N_b} u_{ij}^I x_j^I \tag{14}$$

The corresponding t_i and σ_{ij} can be defined as

$$t_i = \sum_{I=1}^{N_b} t_{ij}^I x_j^I \tag{15}$$

$$\sigma_{ij} = \sum_{I=1}^{N_b} U_{ijk}^I x_k^I \tag{16}$$

where x_j^I are unknown parameters; N_b is the total number of boundary nodes; u_{ij}^I, t_{ij}^I and U_{ijk}^I are the fundamental solutions for 2-D elasticity problem.

V. SYSTEM OF ALGEBRAIC EQUATION

Because the singular fundamental solutions are used in Eqs. (14-16), the integrals in Eqs. (4) and (5) will be singular, as long as the source point s^I is located on the boundary Γ^J of the sub-domain Ω^J centered at the field point s^J (Fig. 2 and Fig. 3). Therefore the singularities may occur, whether s^J and s^I are coincident or not.

It should been pointed out that the integrand of the second integral in Eq. (4) equals zero at any point inside the sub-domain Ω^J or on the boundary Γ^J

except at the source point s^I. In order to evaluate this integral, a circle of radius ε centered at s^I is subtracted from Ω^J. The modified sub-domain with the boundary $\Gamma'^J=\Gamma_c^J\cup\Gamma_\varepsilon^J$ is denoted as Ω'^J. Thus, in the limit as $\varepsilon\to 0$, $\Omega'^J\to\Omega^J$. Eq. (4) holds in Ω'^J:

$$\lim_{\varepsilon\to 0}\int_{\Gamma_\varepsilon^J} t_i v^J d\Gamma + \lim_{\varepsilon\to 0}\int_{\Gamma_c^J} t_i v^J d\Gamma - \lim_{\varepsilon\to 0}\int_{\Gamma_\varepsilon^J} \tilde{t}_i v^J d\Gamma$$

$$- \lim_{\varepsilon\to 0}\int_{\Gamma_c^J} \tilde{t}_i v^J d\Gamma - \lim_{\varepsilon\to 0}\int_{\Omega'^J} \sigma_{ij,j} v^J d\Omega = 0 \qquad (17)$$

Since the source point s^I is outside the sub-domain Ω'^J, the domain integral in the above equation is vanished. The third part also equals zero. Thus, Eq. (17) can be rewritten as:

$$\lim_{\varepsilon\to 0}\int_{\Gamma_\varepsilon^J} t_i v^J d\Gamma + \lim_{\varepsilon\to 0}\int_{\Gamma_c^J} t_i v^J d\Gamma$$

$$= \int_{\Gamma^J} \tilde{t}_i v^J d\Gamma \qquad (18)$$

By substituting Eqs. (7) and (15) into the above equation, one can obtain

$$\sum_{I=1}^{N_b} \left(\lim_{\varepsilon\to 0}\int_{\Gamma_\varepsilon^J} t_{ik}^I v^J d\Gamma + \lim_{\varepsilon\to 0}\int_{\Gamma_c^J} t_{ik}^I v^J d\Gamma\right) x_k^I$$

$$= \sum_{I=1}^{N} \left(\int_{\Gamma^J} \Phi^I(s) v^J d\Gamma\right) \hat{t}_i^I \qquad (19)$$

When s^I is located outside Ω^J, the first limit in Eq. (19) vanishes, and the second integral becomes regular. Otherwise, when s^I is located inside Ω^J, the second integral should be regarded as its Cauchy principal value, and the first limit is similar to the free terms in BEM, i.e.

$$c_{ik}^{JI} = \begin{cases} \lim_{\varepsilon\to 0}\int_{\Gamma_\varepsilon^J} t_{ik}^I v^J d\Gamma & s^I \in \Gamma^J \\ 0 & s^I \notin \Gamma^J \end{cases} \qquad (20)$$

where c_{ik}^{JI} are coefficients depending upon the test function v^J and the geometrical shape of the boundary Γ^J. Therefore, Eq. (19) can be rewritten as:

$$\sum_{I=1}^{N_b} \left(c_{ik}^{JI} + \int_{\Gamma^J} t_{ik}^I v^J d\Gamma\right) x_k^I = \sum_{I=1}^{N} \left(\int_{\Gamma^J} \Phi^I(s) v^J d\Gamma\right) \hat{t}_i^I \qquad (21)$$

The singularity in Eq. (5) is weak and this kind of singular integral can be evaluated by log-weighted Gaussian quadrature. By substituting Eqs. (6) and (14) into Eq. (5), one can obtain

$$\sum_{I=1}^{N_b} \left(\int_{\Gamma^J} u_{ik}^I v^J d\Gamma\right) x_k^I = \sum_{I=1}^{N} \left(\int_{\Gamma^J} \Phi^I(s) v^J d\Gamma\right) \hat{u}_i^I \qquad (22)$$

By using Eqs. (21) and (22) for all boundary nodes, the system of linear algebraic equations can be written in matrix form

$$\boldsymbol{U}\boldsymbol{x} = \boldsymbol{H}\hat{\boldsymbol{u}} \qquad (23)$$

$$\boldsymbol{T}\boldsymbol{x} = \boldsymbol{H}\hat{\boldsymbol{t}} \qquad (24)$$

where

$$U_{ij}^{JI} = \int_{\Gamma^J} u_{ij}^I v^J d\Gamma \qquad (25)$$

$$T_{ij}^{JI} = c_{ij}^{JI} + \int_{\Gamma^J} t_{ij}^I v^J d\Gamma \qquad (26)$$

$$H_{ij}^{JI} = \begin{cases} \int_{\Gamma^J} \Phi^I(s) v^J d\Gamma, & i = j \\ 0, & i \neq j \end{cases} \qquad (27)$$

$$\boldsymbol{x}^T = [x_1^1, x_2^1, \cdots, x_1^{N_b}, x_2^{N_b}] \qquad (28)$$

$$\hat{\boldsymbol{u}}^T = [\hat{u}_1^1, \hat{u}_2^1, \cdots, \hat{u}_1^{N_b}, \hat{u}_2^{N_b}] \qquad (29)$$

$$\hat{\boldsymbol{t}}^T = [\hat{t}_1^1, \hat{t}_2^1, \cdots, \hat{t}_1^{N_b}, \hat{t}_2^{N_b}] \qquad (30)$$

For a well-posed problem, the value of either u_i or t_i is known on the boundary. Before the solution of the problem, the linear equations in (23) and (24) should be rearranged by appropriate switching of rows to make Eq. (23) contain the prescribed boundary conditions and Eq. (24) contain the unknown ones. During the rearrangement, those rows of $\boldsymbol{T}$ and $\hat{\boldsymbol{t}}$ in Eq. (24) related to the prescribed traction boundary conditions are interchanged with the corresponding rows of $\boldsymbol{U}$ and $\hat{\boldsymbol{u}}$ in Eq. (23) related to the unknown displacement boundary conditions, while the other rows do not need such treatment.

After solving the rearranged equations, we can obtain the unknown vector $\boldsymbol{x}$ and the unknowns of $\hat{\boldsymbol{t}}$ and $\hat{\boldsymbol{u}}$. Then, displacements u_i and tractions t_i on the boundary Γ can be evaluated by using the MLS approximation in Eqs. (6) and (7), while displacements u_i and stresses σ_{ij} in the domain Ω can be evaluated by Eqs. (14) and (16), respectively, without further integrations.

VI. TREATMENT OF SINGULAR INTEGRALS

In order to avoid the singular integrals in

HBNM, the RHBNM puts the source points of the fundamental solutions outside the domain. However, such treatment may increase complication in solving problems associated with irregular geometries and destroy the numerical stability some times.

In this section, HBNM will be improved by accurate and appropriate evaluations of the singular integrals referred to BEM (Brebbia *et al.*, 1984; Guiggiani, 1991). In order to be compared with the original RHBNM, this new improved HBNM is named as Singular Hybrid Boundary Node Method (SHBNM).

It has been mentioned above that the singular integral in Eq. (25) is a weak one, and such kind of singular integral can be evaluated by log-weighted Gaussian quadrature as follows:

$$I_1 = \int_{\xi_s}^{\xi^I} \ln r(\xi^I, \xi) g(\xi) d\xi \tag{31}$$

$$I_2 = \int_{\xi^I}^{\xi_e} \ln r(\xi^I, \xi) g(\xi) d\xi \tag{32}$$

where ξ_s and ξ_e stand for the parameter coordinates of the starting point and ending point of local boundary Γ^J; ξ^I is the parameter coordinate of the source point s^I (Fig. 2 and Fig. 3). After transformation, Eq. (31) can be rewritten as:

$$I_1 = \int_0^1 \ln \frac{1}{\eta} f(\eta) d\eta = \sum_{i=1}^{n} w_i f(\eta_i) \tag{33}$$

where

$$f(\eta) = \frac{\ln r(\xi^I, \xi(\eta))}{\ln \frac{1}{\eta}} g(\xi(\eta))(\xi^I - \xi_s)$$

$$\xi(\eta) = (\xi_s - \xi^I)\eta + \xi^I \tag{34}$$

w_i and η_i are the weights and positions of log-weighted Gaussian quadrature. The Eq. (32) can be evaluated in the same way.

The Cauchy principal value of the singular integrals in Eq. (26) and the corresponding coefficients c_{ik}^{JI} can be evaluated using the rigid-body motion approach indirectly. This approach requires only one source point located inside each sub-domain (i.e., the radius r^J should be less than the minimum value of the distances to the adjacent nodes). Fortunately, this restriction affects the accuracy and convergence only a little in the present method. Numerical experiments in the next section will show good numerical results, as long as an appropriate radius r^J is chosen.

Two particular solutions of rigid-body displacements are chosen as:

$$u_1 \equiv 1,\ u_2 \equiv 0,\ t_1 = t_2 \equiv 0$$

$$u_1 \equiv 0,\ u_2 \equiv 1,\ t_1 = t_2 \equiv 0 \tag{35}$$

Thus, $\hat{u}_i^I$ and $\hat{t}_i^I$ can be obtained by using Eqs. (12) and (13):

$$\hat{\boldsymbol{u}}_1^T = [1,\ 0,\ 1,\ 0,\ \cdots,\ 1,\ 0]$$

$$\hat{\boldsymbol{u}}_2^T = [0,\ 1,\ 0,\ 1,\ \cdots,\ 0,\ 1] \tag{36}$$

$$\hat{\boldsymbol{t}}_1 = 0\ ,\ \hat{\boldsymbol{t}}_2 = 0 \tag{37}$$

By substituting Eq. (36) into Eq. (23), we can obtain two unknown vectors $\boldsymbol{a}$ and $\boldsymbol{b}$ as follows:

$$\boldsymbol{a} = \boldsymbol{U}^{-1}\boldsymbol{H}\hat{\boldsymbol{u}}_1$$

$$\boldsymbol{b} = \boldsymbol{U}^{-1}\boldsymbol{H}\hat{\boldsymbol{u}}_2 \tag{38}$$

Substituting Eqs. (37) and (38) into Eq. (24) leads to the evaluation of diagonal components in the matrix $\boldsymbol{T}$:

$$\begin{Bmatrix} T_{i1}^{JJ} \\ T_{i2}^{JJ} \end{Bmatrix} = \begin{bmatrix} a_1^J & a_2^J \\ b_1^J & b_2^J \end{bmatrix}^{-1} \begin{Bmatrix} -\sum_{\substack{I=1 \\ I \neq J}}^{N_b} T_{ik}^{JI} a_k^I \\ -\sum_{\substack{I=1 \\ I \neq J}}^{N_b} T_{ik}^{JI} b_k^I \end{Bmatrix} \tag{39}$$

Similar to the Hybrid BEM, the "boundary layer effect" in HBNM can also be observed, i.e., numerical results evaluated by Eqs. (14-16), on the points close to the boundary depart from the exact solutions. Nevertheless, an alternative approach to evaluate results inside the domain can be proposed referred to BEM:

$$u_i(P) = \int_\Gamma u_{ij}(P; q)\tilde{t}_j(q) d\Gamma - \int_\Gamma t_{ij}(P; q)\tilde{u}_j(q) d\Gamma$$

$$\sigma_{ij}(P) = \int_\Gamma U_{ijk}(P; q)\tilde{t}_k(q) d\Gamma - \int_\Gamma T_{ijk}(P; q)\tilde{u}_k(q) d\Gamma \tag{40}$$

where P denotes the point inside the domain for evaluating variables, and also the source point of the fundamental solution; u_{ij}, t_{ij}, U_{ijk} and T_{ijk} are the fundamental solution for plane strain problem.

The difference of using Eq. (40) for BEM and in the present approach is that the boundary integrals in BEM are evaluated on boundary elements, while these in the present approach are evaluated on the piecewise smooth segments. When the points are close to the boundary, nearly-singular integrals will

occur. To appropriately evaluate such integrals, more integration points or special treatments, such as that presented in (Mukherjee *et al*., 2000) and (Luo, *et al*., 1998), are required.

VII. NUMERICAL EXAMPLES

For the error estimation and convergence investigation, a L_2 norm error is defined as follows:

$$e = \frac{1}{|u|_{\max}} \sqrt{\frac{1}{N} \sum_{i=1}^{N} (u_i^{(e)} - u_i^{(n)})^2} \tag{41}$$

where $|u|_{\max}$ is the maximum value of $u=\sqrt{u_i u_i}$ in the selected N sample points; the exact and numerical solutions are referred by the superscripts (e) and (n) respectively.

In all examples below, the parameters mentioned in Section II and III are chosen as $\hat{d}^I=3.5h$, $\hat{d}^I/c^I=4.0$, $r^J=0.9996d$, $r^J/c^J=0.3$, in which h is mesh size, and d is minimum value of the distances from the current node to the adjacent nodes.

1. Patch Test

The first illustrative example is a Dirichlet problem on a square, which is bounded by the lines $x=0$, $y=0$, $x=1$ and $y=1$, and the exact displacement field is considered as follows:

$$u_1=2x+3y \quad u_2=3x+2y$$

where the displacement boundary condition is prescribed on all the boundary lines according to these equations.

In order to investigate how the radius r^J of the sub-domain affects the accuracy and convergence of the present method, three schemes of regular node arrangements, namely 5, 10 and 20 nodes respectively on each edge, are considered. Since the satisfaction of the patch test requires the displacement inside the domain to be given the same function in the exact displacement field, 15 uniformly spaced sample points on the diagonal from (0.15, 0.85) to (0.85, 0.15) and 19 uniformly spaced sample points on the diagonal from (0.0, 1.0) to (1.0, 0.0) inside the domain are selected. The relative errors of the displacement u_x, stresses σ_x and τ_{xy} on these sample points are shown in Figs. 4(a-b), and the convergence rates of the displacement u_x on these sample points are shown in Fig. 4(c). The comparisons show that the restriction of $r^J<1.0$ affects the numerical results only a little and high accuracy and high convergence rate can be obtained, as long as r^J is chosen appropriately.

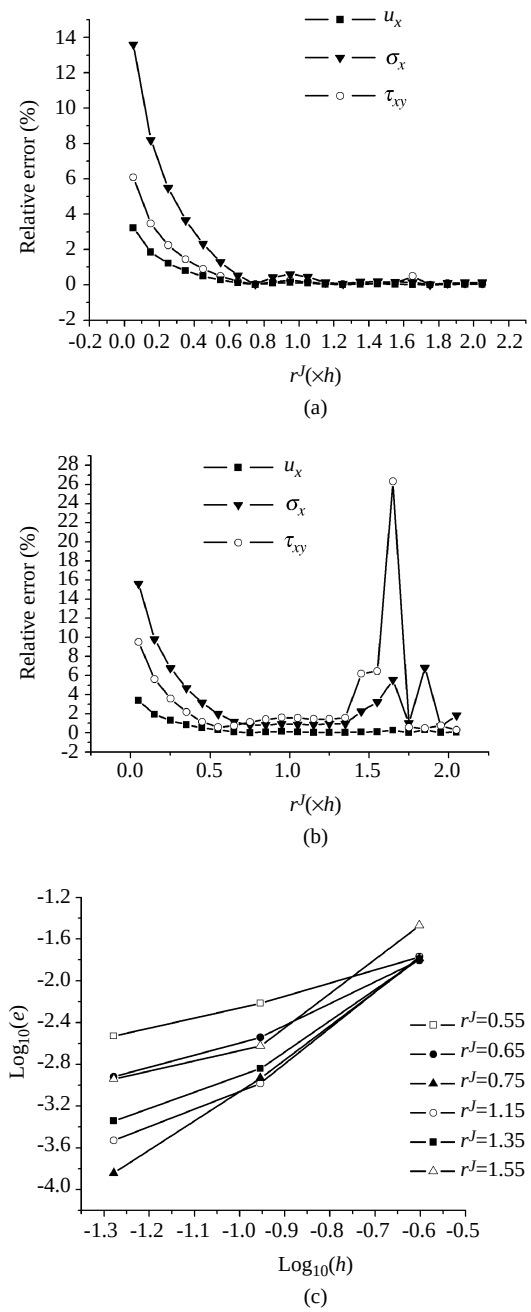

Fig. 4 (a) Relative errors of u_x, σ_x and τ_{xy} inside the domain (15 sample points); (b) relative errors of u_x, σ_x and τ_{xy} inside the domain (19 sample points); (c) convergence rates of u_x inside the domain (19 sample points)

2. Cylindrical Tube Subjected to Uniform Internal Pressure

This problem is the well-known Lamé problem, in which a cylindrical tube with a and b as its inner and outer radii subjected to uniform internal pressure is considered. The plane strain case is considered, and the parameters are chosen as Young's modulus E=25 MPa, Poisson's ratio v=0.3, internal pressure

Table 1 Three schemes of node arrangement

Total number	*AB*	*BC*	*CD*	*DA*
33	6	7	6	14
66	12	14	12	28
99	18	21	18	42

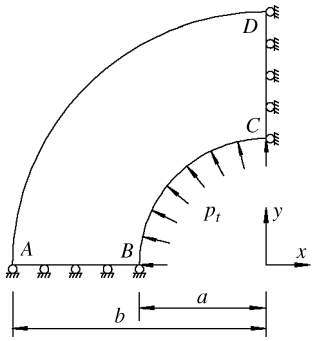

Fig. 5 Model for cylindrical tube subjected to uniform internal pressure

p_i=1 MPa. Fig. 5 shows its geometry with dimension a=100 mm and b=200 mm, and the corresponding boundary conditions are prescribed as follows:

$$\sigma_r=-p_i \quad \tau_{r\theta}=0 \quad \text{on} \quad r=a$$

$$\sigma_r=0 \quad \tau_{r\theta}=0 \quad \text{on} \quad r=b$$

The exact stress fields in polar coordinates are:

$$\sigma_r=\frac{a^2p_i}{b^2-a^2}(1-\frac{b^2}{r^2}) \quad \sigma_\theta=\frac{a^2p_i}{b^2-a^2}(1+\frac{b^2}{r^2})$$

Due to its symmetry, only the upper left quarter requires to be modeled. Three schemes of uniform node arrangement are selected, as listed in Table 1.

The tractions in y direction on the edge AB and the corresponding exact solutions are shown in Fig. 6.

3. An Infinite Sheet with a Hole

In this example, only a portion of an infinite sheet with a central circular hole subjected to a unidirectional tensile load S in the x direction is considered. The analytical solutions of stresses are

$$\sigma_r=\frac{S}{2}(1-\frac{a^2}{r^2})+\frac{S}{2}(1+\frac{3a^4}{r^4}-\frac{4a^2}{r^2})\cos(2\theta)$$

$$\sigma_\theta=\frac{S}{2}(1+\frac{a^2}{r^2})-\frac{S}{2}(1+\frac{3a^4}{r^4})\cos(2\theta)$$

$$\tau_{r\theta}=-\frac{S}{2}(1-\frac{3a^4}{r^4}+\frac{2a^2}{r^2})\sin(2\theta)$$

Table 2 Two schemes of node arrangement

Total number	*AB*	*BC*	*CD*	*DE*	*EA*
74	10	24	20	10	10
58	10	8	20	10	10

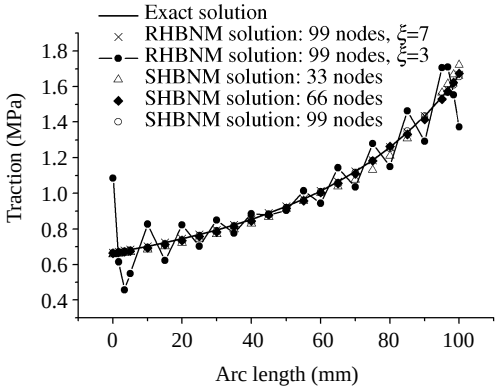

Fig. 6 Traction t_y distribution along edge AB

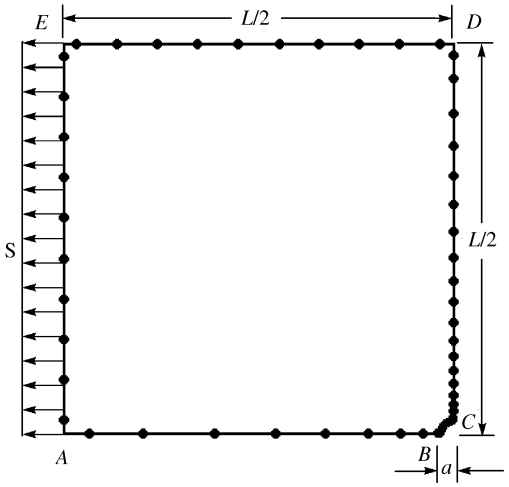

Fig. 7 A quarter of an infinite sheet with a central circular hole subjected to a unidirectional tensile load

The plane stress case is considered, and the parameters here are S=1 MPa, E=25 MPa, v=0.3 (Fig. 7). The length of the sheet L=60 mm is much greater than the radius of the hole a=1 mm, to approximate the infinite sheet. To compare with the original RHBNM, two schemes of non-uniform node arrangements, as listed in Table 2, are adopted.

In RHBNM, all the parameters are chosen the same as the ones in SHBNM, except r^J=3.0h, and the scale factor is taken as ξ=7. The stresses σ_x on the edge CD and the corresponding analytical solutions are shown in Fig. 8. The numerical results of the two approaches both agree excellently with the analytical solution, when 74 nodes are used. It can be observed that, when the number of nodes on edge BC

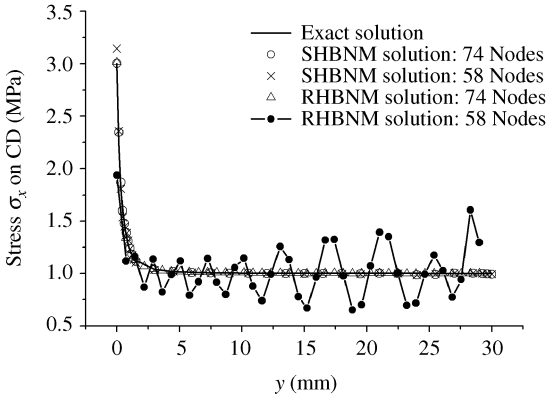

Fig. 8 Stress σ_x distribution along edge *CD*

changes from 24 to 8, the numerical results of stresses σ_x on edge *CD* in RHBNM change significantly; on the contrary, only a little change happens in SHBNM. Therefore, in comparison with the numerical results of the original RHBNM, the SHBNM solution has shown better stability and accuracy.

4. Cantilever Beam

In the final example, a cantilever beam is considered (Fig. 9). The analytical solutions for displacements and stresses are

$$u_x = -\frac{P}{6EI}(y-\frac{h}{2})[3x(2L-x)+(2+\nu)(y^2-hy)]$$

$$u_y = \frac{P}{6EI}[3\nu(L-x)(y^2-hy+\frac{1}{4}h^2)+\frac{4+5\nu}{4}h^2x + 3x^2(L-\frac{1}{3}x)]$$

$$\sigma_x = -\frac{P}{I}(L-x)(y-\frac{1}{2}h)$$

$$\sigma_y = 0$$

$$\tau_{xy} = -\frac{P}{2I}y(y-h)$$

where $I=h^3/12$.

The parameters are E=30 MPa, ν=0.3, P=1 N. The geometry of the beam with dimension L=4 m and h=1 m is shown in Fig. 9. A uniform arrangement of 120 nodes (10 nodes on *AD* and *BC* each, 50 nodes on *AB* and *CD* each) is chosen. In order to compare with the original RHBNM, two types of boundary conditions are considered:

$$\text{BC1:}\begin{cases} u_x = 0 \\ u_y = 0 \end{cases}$$

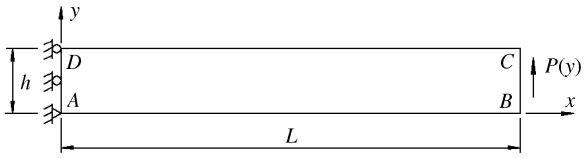

Fig. 9 Cantilever beam

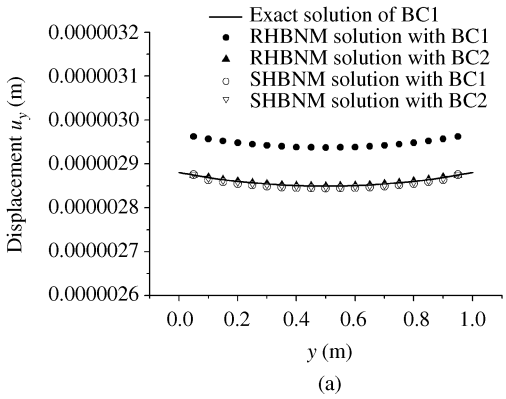

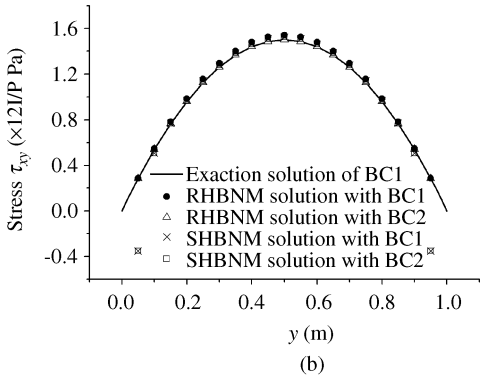

Fig. 10 (a) Displacement u_y distribution at $x=L/2$; (b) stress τ_{xy} distribution at $x=L/2$

$$\text{BC2:}\begin{cases} u_x = -\dfrac{P(2+\overline{\nu})}{6\overline{E}I}(y-\dfrac{h}{2})(y^2-hy) \\ u_y = \dfrac{P\overline{\nu}L}{2\overline{E}I}(y^2-hy+\dfrac{1}{4}h^2) \end{cases}$$

In RHBNM, the scale factor is taken as ξ=7, and all other parameters are chosen the same as those in SHBNM. The comparisons of the shear stress τ_{xy} for 19 uniformly spaced sample points from (2.0, 0.15) to (2.0, 0.85), and displacements u_y for 21 uniformly spaced sample points from (2.0, 0.0) to (2.0, 1.0), together with the exact solution of BC1, are shown in Fig. 10.

It can be observed that, when the boundary conditions change a little, the numerical results change much in RHBNM, while almost no change happens in the numerical results of SHBNM. Thus,

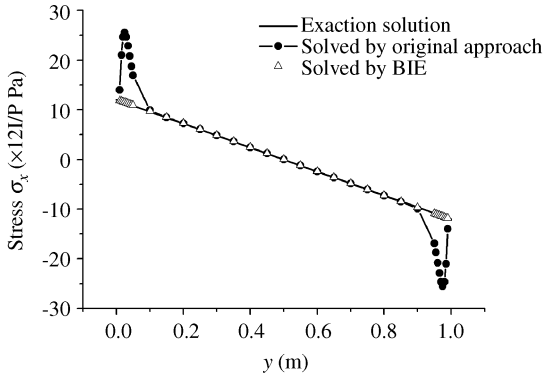

Fig. 11 Stress σ_x distribution at $x=L/2$

the numerical stability of RHBNM is not as good as that of SHBNM.

Since more attention should be paid to the "boundary layer effect", the SHBNM solutions with BC1 of stress σ_x evaluated by Eqs. (16) and (40) are both shown in Fig. 11. From the comparison, we can see that the "boundary layer effect" can be properly treated by appropriate evaluations of the integrals in Eq. (40). Therefore, values close to the boundary can be evaluated by the Boundary Integral Eq. (40), and others can be evaluated easily by original treatment, i.e., Eqs. (14-16).

VIII. CONCLUDING REMARKS

In this paper, a new singular scheme of meshless HBNM for 2-D elastostatics is presented. By appropriate evaluation of singular integrals, SHBNM possesses better numerical stability and more convenience to solve complicated problems, especially involving irregular geometry, than the original RHBNM, while the guarantee of the numerical precision is a prerequisite. Since it has the advantages of both BEM and truly meshless methods, SHBNM is appropriate for solving problems associated with moving contact boundaries or crack propagation. Similar to other meshless methods, some problems, such as the drawback of serious "boundary layer effect", in SHBNM still require further investigation.

ACKNOWLEDGMENTS

The research is supported by the Special Foundation for the Authors of the Nationwide (China) Excellent Doctoral Dissertation (Project no: 200242).

REFERENCES

Atluri, S. N., Kim, H. G., and Cho, J. Y., 1999, "A Critical Assessment of the Truly Meshless Local Petrov-Galerkin (MLPG), and Local Boundary Integral Equation (LBIE) Methods," *Computational Mechanics*, Vol. 24, No. 5, pp. 348-372.

Atluri, S. N., and Shen, S. P., 2002, *The Meshless Local Petrov-Galerkin (MLPG) Method*, Technical Science Press, USA.

Atluri, S. N., Sladek, J., Sladek, V., and Zhu, T., 2000, "The Local Boundary Integral Equation (LBIE) and it's Meshless Implementation for Linear Elasticity," *Computational Mechanics*, Vol. 25, Nos. 2-3, pp. 180-198.

Atluri, S. N., and Zhu, T., 1998, "A New Meshless Local Petrov-Galerkin (MLPG) Approach in Computational Mechanics," *Computational Mechanics*, Vol. 22, No. 2, pp. 117-127.

Atluri, S. N., and Zhu, T., 2000, "The Meshless Local Petrov-Galerkin (MLPG) Approach for Solving Problems in Elasto-Statics," *Computational Mechanics*, Vol. 25, Nos. 2-3, pp. 169-179.

Belytchko, T., Krongauz, Y., Organ, D., Fleming, M., and Krysl, P., 1996, "Meshless Methods: An Overview and Recent Developments," *Computer Methods in Applied Mechanics and Engineering*, Vol. 139, No. 1-4, pp. 3-47.

Belytschko, T., Lu, Y. Y., and Gu, L., 1994, "Element Free Galerkin Methods," *International Journal for Numerical Methods in Engineering*, Vol. 37, No. 2, pp. 229-256.

Brebbia, C. A., Telles, J. C., and Wrobel, L. C., 1984, *Boundary Element Techniques*, Springer Verlag, Berlin, Germany.

DeFigueredo, T. G. B., and Brebbia, C. A., 1989, "A New Hybrid Displacement Variational Formulation of BEM for Elastostatics," *Advances in Boundary Elements*, C. A. Brebbia and J. J. Conner ed., Computational Mechanics Publications, Southampton, Vol. 1, pp. 47-57.

Guiggiani, M., 1991, "The Evaluation of Cauchy Principal Value Integrals in the Boundary Element Method-a Review," *Mathematical and Computer Modelling*, Vol. 15, Nos. 3-5, pp. 175-184.

Kothnur, V. S., Mukherjee, S., and Mukherjee, Y. X., 1999, "Two-Dimensional Linear Elasticity by the Boundary Node Method," *International Journal of Solids and Structures*, Vol. 36, No. 8, pp. 1129-1147.

Liu, W. K., Jun, S., and Zhang, Y. F., 1995, "Reproducing Kernel Particle Methods," *International Journal for Numerical Methods in Fluids*, Vol. 20, Nos. 8-9, pp. 1081-1106.

Lucy, L. B., 1977, "A Numerical Approach to the Testing of the Fission Hypothesis," *The Astronomy Journal*, Vol. 8, No. 12, pp. 1013-1024.

Luo, J. F., Liu, Y. J., and Berger, E. J., 1998, "Analysis of Two-Dimensional Thin Structures (from Micro- to Nano-Scales) Using the Boundary

Element Method," *Computational Mechanics*, Vol. 22, No. 5, pp. 404-412.

Mukherjee, Y. X., and Mukherjee, S., 1997, "The Boundary Node Method for Potential Problems," *International Journal for Numerical Methods in Engineering*, Vol. 40, No. 5, pp. 797-815.

Mukherjee, S., Chati, M. K., and Shi, X., 2000, "Evaluation of Nearly Singular Integrals in Boundary Element Contour and Node Methods for Three-Dimensional Linear Elasticity," *International Journal of Solids and Structures*, Vol. 37, No. 51, pp. 7633-7654.

Nayroles, B., Touzot, G., and Villon, P., 1992, "Generalizing the Finite Element Method: Diffuse Approximation and Diffuse Element," *Computational Mechanics*, Vol. 10, pp. 307-318.

Wu, Z., 1995, "Compactly Supported Positive Definite Radial Functions," *Advances in Computational Mathematics*, Vol. 4, pp. 283-292.

Zhang, J. M., and Yao, Z. H., 2001a, "Meshless Regular Hybrid Boundary Node Method," *Computer Modeling in Engineering and Sciences*, Vol. 2, No. 3, pp. 307-318.

Zhang, J. M., and Yao, Z. H., 2001b, "A New Meshless Regular Hybrid Boundary Node Method," *Proceedings of the 1st MIT Conference on Computational Fluid and Mechanics*, K. J. Bathe ed., Vol. 2, pp. 1680- 1682.

Zhang, J. M., and Yao, Z. H., 2002, "Analysis of 2-D Thin Structures by the Meshless Regular Hybrid Boundary Node Method," *Acta Mechanica Solida Sinica*, Vol. 15, No. 1, pp. 36-44.

Zhang, J. M., Yao, Z. H., and Li, H., 2002, "A Hybrid Boundary Node Method," *International Journal for Numerical Methods in Engineering*, Vol. 53, No. 4, pp. 751-763.

Zhang, J. M., Yao, Z. H., and Tanaka, M., 2003, "The Meshless Regular Hybrid Boundary Node Method for 2D Linear Elasticity," *Engineering Analysis with Boundary Elements*, Vol. 27, No. 3, pp. 259-268.

Zhang, J. M., and Yao, Z. H., 2004, "The Regular Hybrid Boundary Node Method for Three-Dimensional Linear Elasticity," *Engineering Analysis with Boundary Elements*, Vol. 28, No. 5, pp. 525-534.

Zhu, T., Zhang, J., and Atluri S. N., 1998, "A Local Boundary Integral Equation (LBIE) Method in Computational Mechanics, and a Meshless Discretization Approach," *Computational Mechanics*, Vol. 21, No. 3, pp. 223-235.

Manuscript Received: Jul. 04, 2003
Revision Received: Dec. 03, 2003
and Accepted: Dec. 22, 2003